07

# Broadband infrared radiation detector based on laser-induced graphene

© Yu.P. Sukhorukov,[1] A.V. Telegin,[1] R.G. Zonov,[2] G.M. Mikheev[2]

[1]M.N. Mikheev Institute of Metal Physics, Ural Branch, Russian Academy of Sciences, Yekaterinburg, Russia
[2]Udmurt Federal Research Center, Ural Branch Russian Academy of Sciences, Izhevsk, Russia
e-mail: telegin@imp.uran.ru

*Received July 25, 2025*
*Revised October 1, 2025*
*Accepted October 8, 2025*

A broadband high-frequency infrared radiation detector based on laser-induced graphene (LIG) obtained by pyrolysis of a polyimide film has been developed. The spectral characteristic of the detector's photoresponse corresponds to the spectrum of an absolute blackbody, except for features inherent to the setup. Unlike standard bolometers, the frequency dependence of the laser-induced graphene-based detector is determined by two different mechanisms. This results in a weak loss of the detector's sensitivity at frequencies up to and higher $1-10$ kHz. The detector's efficient light absorption across a broad spectral range (from $1 < \lambda < 21\,\mu$m) under various conditions and its relatively high sensitivity ($\sim 0.16$ %/W) make it a promising candidate for the development of technologically simple and cost-effective infrared receivers.

**Keywords:** laser-induced graphene, infrared range, bolometric receiver, polyimide film, high-frequency modulation.

DOI: 10.61011/TP.2026.03.63168.197-25

## Introduction

In the recent two decades, physical and chemical properties have been extensively studied and physical principles of industrial application of graphene have been developed [1–3]. Unique properties of graphene such as the absence of band gap, high charge carrier mobility and transparency, high thermal and electric conductivity, and low heat capacity stimulate the studies in the area of transport and photoinduced phenomena [4–8]. For example, special focus is made on creating thermal imaging cameras, electromagnetic radiation processing and conversion devices, focal plane matrices, etc. [7,9–12]. Principle of operation of such devices is predominantly based on varying the electrical resistance of graphene through heating by electromagnetic radiation. Low heat capacity and high thermal conductivity of graphene theoretically provide fast response at frequencies close to the terahertz range ($\sim 10^{12}$ Hz) [7–10]. However, creation of monolayer graphene photodetectors faces significant restrictions: firstly, the proportion of incident radiation absorption is extremely small ($\sim 2\%$ [6,12]) and, secondly, when graphene is used a photoresist, high dark current density is observed in the electric circuit, thus, reducing the signal-to-noise ratio and device sensitivity.

Various graphene structures can serve as a potential solution of the problem. In such three-dimensional ($3D$) structures, effective surface and, consequently, proportion of absorbed light increase many-fold, and multiple randomly connected graphene monolayers make it possible to distribute electric current between them and reduce current density in contacts [10,12–14]. Direct laser destructuring (pyrolysis) of polyimide films leading to formation of laser-induced graphene (LIG) is a promising method for synthesizing such structures [15]. LIG is a highly porous conducting $3D$-carbon material consisting of nanoscale fragments of graphene-like layers randomly oriented in a three-dimensional matrix with a lot of defects and pores [15]. Strictly speaking, LIG is not classified either as classical $2D$-graphene or as ordered graphite [16]. However, LIG is a well-established term that is widely used in the literature on laser pyrolysis of various carbon-containing precursors. Simplicity and high rate of LIG film production have resulted in extensive development of various LIG-based sensors [17–25], microfluidic devices [26–32], memory devices [33–40], ecosystem smart devices [26,28,41–45], etc. Large thickness of LIG films ($d \sim 20-300\,\mu$m [13,46,47]) provides high light absorption coefficients, electrical resistances and capacities [45,48–50]. Thus, a photodetector with frequency characteristics similar to semiconductor counterparts has been successfully created [32,51], drag effect has been detected during LIG film exposure to nanosecond laser pulses [47], and visible and near-infrared (IR) detector has been proposed [52]. The papers listed above prove a high technological capacity of LIG, in particular, for photonics. Despite these successful efforts, mid-IR LIG detectors haven't been studied in detail.

This paper briefly describes the study of spectral and frequency characteristics of near-IR and mid-IR LIG-film photodetector ($1 < \lambda < 21\,\mu$m) compared with an ideal bolometer, and determines LIG detector sensitivity to incident radiation intensity.

## 1. Samples and experiment conditions

LIG is a highly porous conducting 3*D*-structure with a specific surface up to several hundreds of $m^2/g$ consisting of turbostratic graphite nanocrystallites randomly oriented relative to each other [53]. LIG was synthesized in air in normal conditions via laser pyrolysis of carbon-containing precursor in the form of 125 $\mu$m polyimide film. An IR radiation detector (inset in Figure 1, *a*) was made on the polyimide film surface through line-by-line scanning by focused continuous gas ($CO_2$) laser ($\lambda = 10.6\,\mu$m) in a predetermined path [13,54]. Laser radiation parameters were controlled using the PM100D power meter coupled with the S425C-L thermal power sensor. Laser beam diameter, laser power, scanning rate and line spacing were 190 $\mu$m, 6 W, 220 mm/s and 25 $\mu$m, respectively. It should be noted that continuous and pulsed lasers, including femtosecond laser complexes, are used for LIG synthesis and for various carbon material modification applications [15,55–58]. Laser power (peak pulsed power) and radiation wavelength (defining the photon energy and material's absorption factor) are important variables in this case. This study uses $CO_2$ laser radiation that is effectively absorbed by the polyimide film. Due to this a more uniform LIG structure can be synthesized [59,60]. From a practical standpoint, it is also essential that continuous carbon dioxide lasers ($CO_2$ lasers) feature relatively low cost and ease of operation.

Meander-shaped samples (LIG detectors) with a total length of 85 mm, line width and thickness 300 and 20 $\mu$m, respectively, were prepared via laser thermal treatment of the polyimide film. Meander ends had $2 \times 2$ mm contact pads. Exposed meander surface was $5 \times 8$ mm. Due to mechanical and physical properties (flexibility) of the polyimide film (substrate), LIG samples made on the film surface are also flexible, which was also found in other works (see, for example, [60–62]).

Figure 1, *a* shows a LIG surface fragment image made using a scanning-electron microscope (SEM) (Thermo Fisher Scientific Quattro S).

It can be seen that the synthesized material has a spongy structure consisting of interlaced networks of open cavities with various shapes and sizes, and lamellar formations with various orientation. Raman scattering spectrum of the LIG film surface measured via excitation by 632.8 nm helium-neon laser radiation on the HORIBA HR800 spectrometer is shown in Figure 2, *b*.

The shown spectrum consists of four well-known Raman bands *D*, *G*, *D′* and 2*D* described in many studies of LIG synthesis [13–18]. Besides these four bands, band $D + D'$ is clearly displayed in the high frequency shift region [53]. Similar Raman bands have defect graphene, graphite crystallites with defects, and turbostratic graphite nanocrystallites. Analysis of the ratio of the above-mentioned band areas to the *G*-band area, and of their frequency position, width and line shapes proves that LIG consists of turbostratic graphite nanocrystallites with

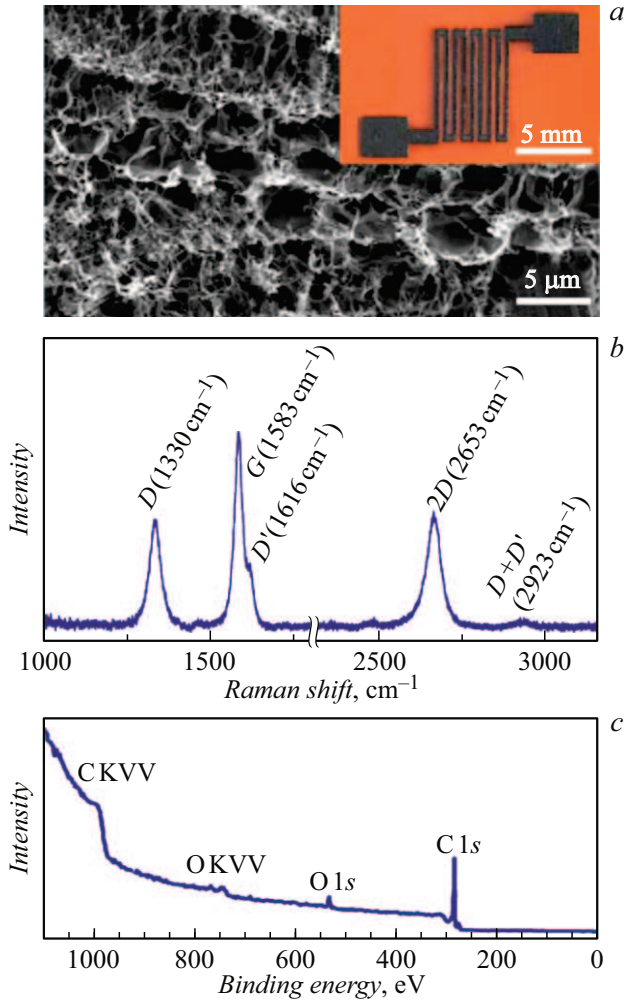


**Figure 1.** SEM image of the LIG surface (*a*) (inset shows a photograph of a meander-shaped LIG detector), Raman scattering spectrum (*b*) and panoramic XPS spectrum of the LIG surface (*c*).

a size of crystallites along the graphene layer plane of about 16 nm. Chemical state analysis of LIG used the X-ray photoelectron spectrometry (XPS) technique (SPECS spectrometer, Surface Nano Analysis GmbH). Figure 2, *c* shows a panoramic XPS spectrum, which is typical of LIG synthesized in the above-mentioned conditions of laser pyrolysis of polyimide film. It can be seen that the spectrum contains oxygen line O1s in addition to carbon line C1s. Detailed examination of XPS spectra indicates that the LIG surface also has trace concentrations of nitrogen. Processing of the measured XPS spectrum shows that concentrations of carbon, oxygen and nitrogen are 87.6 at.%, 11.1 at.% and 0.6 at.%, respectively. Decomposition of spectra C1s and O1s demonstrates that the LIG surface contains oxygen-containing and nitrogen-containing groups ($C-O$, $C=O$, $O-C=O$, $C-N$, etc.), which can affect optical and electrical properties of LIG. Dark resistance of the meander $R$ is $\sim 5\,$k$\Omega$ (resistivity $\rho \sim 0.075\,\Omega\cdot$cm) at room temperature ($T = 295\,$K), which corresponds to graphene

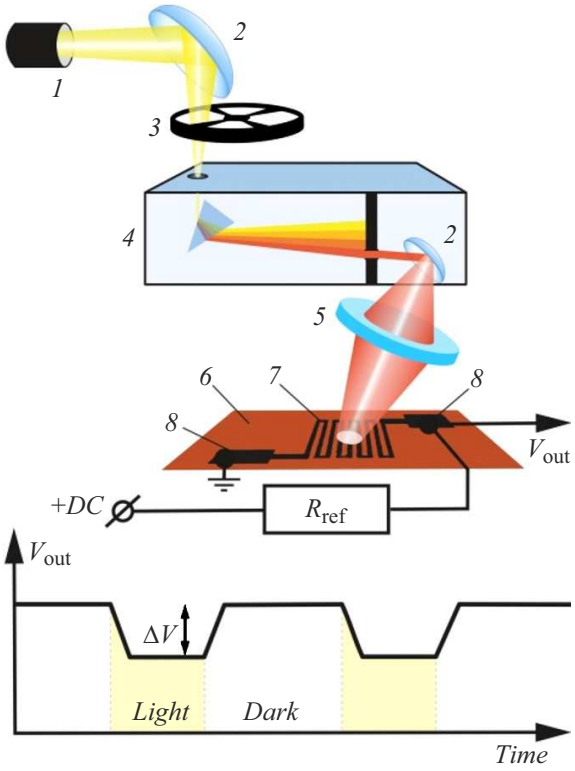


**Figure 2.** Experiment setup: *1* — globar, *2* — parabolic mirror, *3* — mechanical shutter, *4* — monochromator, *5* — KBr lens, *6* — polyimide film, *7* — meander-shaped LIG detector on the polyimide film surface, *8* — contact pads. Schematic diagram of the LIG detector photoresponse is shown at the bottom of the figure.

resistivities in [8,63]. In formal approximation of LIG in the form of conducting homogeneous graphene film, the maximum mid-IR skin layer thickness ($\delta$) can be estimated as $\delta = 2\rho\lambda/\mu_0 c^{1/2} \sim 5.4\,\mu$m at $\lambda = 20\,\mu$m ($\mu_0$ is the magnetic constant, $c$ is the speed of light in vacuum). This quantity shows the mean depth to which the field penetrates the LIG structure at low frequencies (RF and microwave frequencies), where the skin effect prevails over the dielectric loss. Light absorption by the graphene grid itself and scattering on pores prevail at high frequencies (optics, IR). In this case, the light penetration depth $\delta_{opt}$ is mainly defined by the macroscopic absorption coefficient of the structure $\delta_{opt} = \lambda/4\pi k$, where $k$ is the extinction coefficient, which depends on the graphene concentration, pore morphology, wavelength, light interference within the structure, etc. Generally, $\delta_{opt}$ is much smaller than $\delta$. Since the estimated thickness of synthesized LIG ($d = 20\,\mu$m) exceeds $\delta$ ($d > \delta > \delta_{opt}$), then in our case almost full absorption of incident IR radiation is provided in the operating spectral range at room temperature.

Three types of connections between LIG and conducting silver wires were used for fabricating electrical contacts of the meander: 1) Kontaktol type conductive Ag-based adhesive; 2) In melt; 3) Cu film. All contacts had equivalent properties during two to three weeks. Type 1 and 2 contacts further demonstrated the signs of degradation. Therefore, the study used more stable $\sim 200$ nm copper contacts formed by magnetron sputtering in vacuum at the substrate temperature $T \sim 200\,^\circ$C.

Measurements of photoresponse voltage $\Delta V$ induced by IR radiation in the LIG detector (meander) were performed using a setup described below (Figure 2). Globar (a silicon carbide emitter with an operating temperature of $\sim 1380\,^\circ$C) light modulated by a mechanical shutter (Thorlabs MC2000B) with a frequency up to 10 kHz was focused by a parabolic Al mirror to the entrance slit of the modernized IKS-21M prism IR monochromator. Monochromatic nonpolarized light within $0.5 < \lambda < 21\,\mu$m was focused by the parabolic mirror and KBr lens onto an exposed meander surface in the form of a $\sim 4$ mm spot.

Photoresponse voltage $\Delta V$ was determined as variation of electrical resistance ($\Delta R$) of the LIG detector as a result of its heating to $\Delta T$ with light absorption in accordance with expression [64]:

$$\Delta V = I_{dc}\Delta R = I_{dc}(dR/dT)\Delta T, \qquad (1)$$

where $I_{dc} = U_{dc}/(R_{ref} + R_d)$ is the current at the detector, $U_{dc} = 9\,V$ is the DC power supply voltage, $R_{ref}$ is the load resistance equal to the meander dark resistance (see above), $R_d$ is the exposed meander resistance.

$\Delta V$ was recorded using the Stanford Research SR810 lock-in amplifier and a handmade broadband pre-amplifier. It should be noted that a sufficiently high current density ($\sim 10^2 - 10^3$ A/cm$^2$) didn't lead to any noticeable failure of contacts and sample or a change in the detector's resistive properties. Such thermal stability of the meander can be explained by a many-fold increase in the LIG structure area (number of contacts) compared with monolayer graphene [13,49]. Frequency properties of the LIG detector were measured using a LED with $\lambda = 0.63\,\mu$m in constant or pulsed (square meander) modes with voltage applied from the AKIP-2141 high frequency generator.

## 2. Experimental results

Spectral dependence of the LIG detector photoresponse $\Delta V(\lambda)$ was measured in a wavelength range of $0.5 - 21\,\mu$m at the IR radiation modulation frequency $f = 9.1$ Hz, at which $\Delta V$ reaches its maximum values [52,64] (Figure 3).

In addition, $f = 9.1$ Hz falls within the operating frequency range of a Bi bolometer with a KBr window, thus providing further comparison of the LIG detector variables with the standard IR monochromator detector data.

Spectrum $\Delta V$ for the LIG detector demonstrates its maximum at $\lambda_{max} \approx 1.75\,\mu$m (Figure 3). According to Wien's displacement law ($\lambda_{max} \cdot T = 2898\,\mu$m·K), this position corresponds to a blackbody (BB) temperature $T \approx 1656$ K, which is close to the operating temperature of the globar in the system. For comparison, Figure 3 shows the spectral

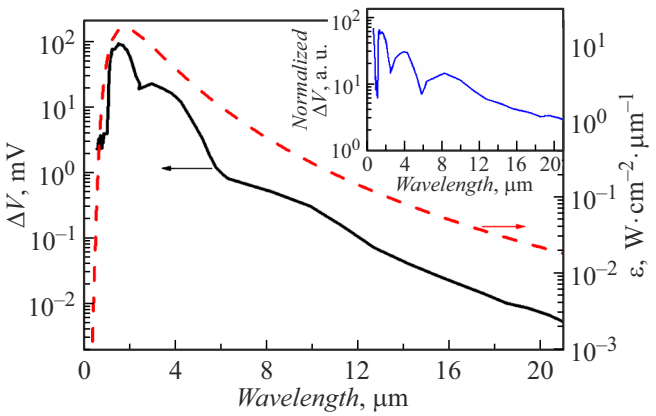


**Figure 3.** Photoresponse spectrum ($\Delta V$) of the LIG detector at $f = 9.1$ Hz (left-hand y axis) and BB radiation spectrum ($\varepsilon$) (right-hand axis) at $T = 1653$ K. The inset shows the LIG detector photoresponse spectrum normalized to the BB spectrum.

dependence of the BB thermal radiant exitance density at $T = 1656$ K calculated using the Planck equation [65]:

$$\varepsilon(\lambda, T) = \frac{2\pi hc^2}{\lambda^5} \cdot \frac{1}{e^{hc/kT\lambda} - 1}, \qquad (2)$$

where $h$ is Planck's constant.

Note that, unlike, for example, photon detectors (InSb, HgCdTe), the LIG detector photoresponse spectrum adequately follows the BB spectrum, which is typical for thermal detectors and provides correct measurements of integral radiation power in a wide IR range without distortions due to inherent spectral selectivity. In a long-wavelength region ($\lambda > 21\,\mu$m), $\Delta V(\lambda)$ spectrum is limited by light absorption by the KBr lens. Sharp decrease in $\Delta V(\lambda)$ in a short-wavelength region ($\lambda < 1.7\,\mu$m) is induced by sharp decrease in the intensity in the BB radiation spectrum. Singularities on curve $\Delta V(\lambda)$ in the $1 - 6\,\mu$m region are associated with IR radiation absorption by atmospheric $H_2O$ and $CO_2$ vapors [66]. Smearing of these singularities is caused by a large spectral slit width ($\Delta\nu$) of the IKS-21M prism monochromator in the experiment. Inset in Figure 3 demonstrates a LIG detector photoresponse spectrum, which, after normalization to the BB spectrum, resembles or is close to the ideal photoresist spectrum. As can be seen from the figure, after such processing, lines related to absorption of $H_2O$ and $CO_2$ vapors are enhanced and $\Delta V$ decreases. Note that a weak monotonic decay of $\Delta V$ with an increase in the light wavelength is caused by nonlinear dispersion of the refractive indices $dn/d\lambda$ of the used replacement glass, NaCl and KRS-5 prisms [56].

Comparative evaluation of the photoresponse of the fabricated LIG detector was performed using a factory-made Bi bolometer from the IKS-21M monochromator with the detectability $D = 10^9 - 10^{10}$ Hz$^{1/2}$·cm/W at room temperature. Comparison has shown that, in the same experiment conditions, photoresponse of the uncooled metal bolometer at 9.1 Hz is only $\sim 10^2 - 10^3$ time higher than that of the LIG detector. Thus, to a rough approximation, the detectability of the fabricated LIG detector is $D \sim 10^6$ Hz$^{1/2}$·cm/W. Additional investigations are required to determine $D$ for LIG more accurately.

Previous [52] and our investigations have shown that only a part of the LIG film participates in electromagnetic energy conversion because the effective skin layer thickness is smaller than the LIG film thickness. Consequently, thickness of the LIG structure itself can be one of the methods of increasing $D$ for the LIG detector because the major proportion of light energy is absorbed in surface layers. In this case, the detector noise shall be also reduced due to an increase in the energy concentration. Note that at this stage in the current experiment conditions and for these LIG samples, the thermal noise is quite high and accurate determination of the thermal noise (or, for example, of detector noise equivalent power (NEP)) seems to be not realistic and not reasonable.

When comparing with the industrial bismuth (Bi)-based bolometer, the LIG detector demonstrates unusual behavior of the dependence of photoresponse $\Delta V(f)$ on light modulation frequency. Figure 4, *a* shows a low-frequency segment of this dependence ($6 < f < 45$ Hz) for LED radiation ($\lambda = 0.63\,\mu$m) modulated using the mechanical shutter.

The presence of a „plateau" on curve $\Delta V(f)$ at $f \leq 10$ Hz and a sharp decrease in sensitivity at high frequencies indicates a bolometric nature of photoresponse in this frequency range. Frequency evaluation of the $\Delta V$ maximum for the bolometer using expression $f_t = 1/\tau$ gives $f_t \approx 5$ Hz, where $\tau \approx C/G$ [54], $C \approx 12$ J/(mol·K) is the heat capacity of graphene at $T = 300$ K [1], $G \approx 5000$ W/(m·K) is the thermal conductivity of graphene [68,69]. Divergence from the experimentally observed frequency of the $\Delta V$ maximum can be attributed to the absence of accurate heat capacity and thermal conductivity data for porous LIG. At the same time, high porosity (more than 90 %) and low density (according

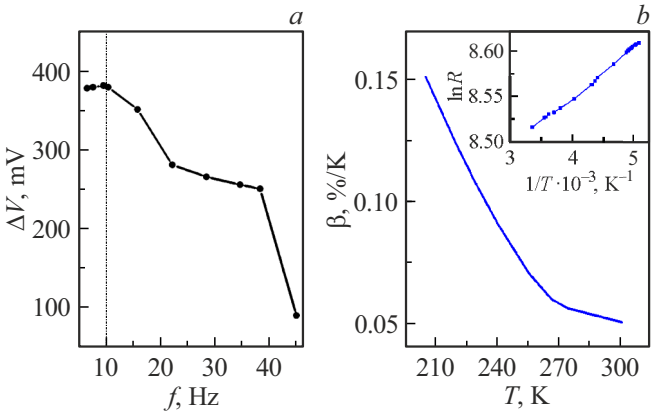


**Figure 4.** *a* — frequency dependence of photoresponse ($\Delta V$) for the LIG detector at $\lambda = 0.63\,\mu$m; *b* — temperature dependence of the thermal resistance coefficient of LIG ($\beta$). The inset shows the reciprocal temperature dependence of the LIG detector resistance.

to various data, from $\sim 4\,\text{mg/cm}^3$ [9] to $\sim 70\,\text{mg/cm}^3$ [13]) lead to a decrease in heat capacity of the LIG detector and, consequently, to an increase in its fast response compared with a bolometer. Note that a decrease in the structure thickness (LIG weight) shall also reduce thermal inertia and increase the LIG detector response rate.

Thermal electric resistance coefficient $\beta = 1/R \cdot dR/dT$, characterizing relative variation of resistance $R$ of the sensing element during heating is an essential variable for bolometer-type detectors. $\beta$ defines the detector sensitivity to temperature variations, i.e. its detectability. For the purpose of this study, $\beta$ was calculated by the slope of $R(T)$ within $200 - 300\,\text{K}$ and was equal to $\beta \approx 0.05\,\%/\text{K}$ at $T = 293\,\text{K}$ and to $\beta \approx 0.15\,\%/\text{K}$ at $T = 200\,\text{K}$ (Figure 4, *b*), which adequately agrees with data for other semiconductors.

The inset in Figure 4, *b* demonstrates that the temperature dependence of the LIG's electrical resistance is adequately described by $\ln R = \ln R_0 + E_a/2kT$, where the carrier activation energy $E_a \sim 5\,\text{meV}$, $R_0 = 5\,\text{k}\Omega$, $k$ is the Boltzmann constant. Semiconductor behavior of $\ln R$ can be attributed to a high defect level of LIG. For example, to adsorption processes and the presence of various functional carbon and oxygen groups in the porous LIG [20–23,52–63], which agrees with the data concerning the graphene band structure modification via chemical functionalization [13–18,63]. Similar behavior of $\beta(T)$ and $R(T)$ is also inherent in graphene oxide and multilayer graphene films fabricated via the aerogel process [8,9]. Note that classical graphene has a „metallic behavior" of $\beta(T)$ and $R(T)$ (see, for example, [2,70]). Thus, the porous structure of LIG and the presence of functional groups lead to detector degradation in atmospheric conditions and appearance of a semiconductor band gap in the spectrum. To stabilize the LIG detector photosensitivity variables and increase $\beta$, LIG synthesis technique can be varied [13–18,27–29,48,49] or various active impurity groups, for example, metal nanoparticles, can be used [4,20,40–42,51].

Figure 4 shows that the bolometric effect in the LIG detector is maintained up to $f = 45\,\text{Hz}$, at which $\Delta V$ is almost four times lower than at the maximum (Figure 3, *a*). With further increase in light modulation frequency, curve $\Delta V(f)$ demonstrates a kink and the signal smoothly decays to $f = 10\,\text{kHz}$ (Figure 5). As reported in [47,48,51], the presence of this component $\Delta V(f)$ can be associated with a so-called „photogating" effect — a kind of photoelectromagnetic EMF induced by variation of free carrier (holes and electrons) mobility and concentration during light absorption process [7,71] in graphene structures. This effect weakly depends on frequency and is associated with unique properties of 2*D*-graphene (including LIG), including low heat capacity, weak electron-phonon interaction, high conductivity ($\sigma \approx 10\,\Omega^{-1}\cdot\text{cm}^{-1}$ [72]) and high carrier mobility. Carrier mobility in the test sample measured with an accuracy to a constant in a standard circuit with four Hall contacts in the meander area was equal to $\mu \sim 4300\,\text{cm}^2/(\text{V}\cdot\text{s})$ at room temperature. This is much lower that in graphene, which can be attributed to the effect

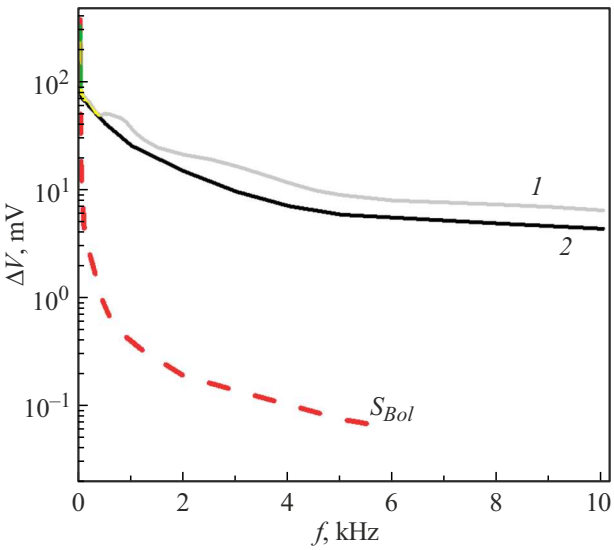


**Figure 5.** Frequency dependence of LIG detector photoresponse ($\Delta V$) with modulation of the LED radiation $\lambda = 0.63\,\mu\text{m}$ by the mechanical shutter (curve *1*) and high frequency generator(curve *2*). For comparison, the dashed line shows the sensitivity curve of an ideal bolometer ($S_{\text{Bol}}$) calculated using expression (4).

of impurities, defects or absorbed molecules. Nevertheless, a LIG THz thermodetector was described in [47], indicating that the LIG detector frequency range can be potentially extended.

Frequency dependence of the LIG detector $\Delta V(f)$ (Figure 5) was studied during exposure to $0.63\,\mu\text{m}$ light. Two methods were used for LED radiation modulation: 1) mechanical–optomechanical shutter with a disc and 2) high frequency electric generator. At modulation frequencies $f < 0.5\,\text{kHz}$, values of $\Delta V$ for both cases almost coincide. LIG detector sensitivity to radiation modulated by the mechanical shutter within $1 < f < 10\,\text{kHz}$ was $\sim 20\,\%$ higher than that in modulation via the electric generator. Such divergence can be attributed to unaccounted relaxation processes in the electronic circuit of signal acquisition from the LIG detector because when radiation intensity is modulated by a sinusoidal waveform, rather than by a square waveform, the difference in $\Delta V(f)$ for both modulation types decreases. Thus, the LIG detector allows good reproduction of pulse waveforms at frequencies up to $f = 10\,\text{kHz}$ (not shown).

Compare experimental dependence $\Delta V(f)$ for the LIG detector with a frequency dependence of the ideal bolometer photosensitivity $S_{\text{Bol}}(f)$ [52]:

$$S_{\text{Bol}} \approx 3U_s\beta/(fC), \tag{3}$$

where $U_s = 9\,\text{V}$ is the bias voltage, $C = 12\,\text{J}/(\text{mol}\cdot\text{K})$ is the LIG heat capacity, $\beta = 0.05\,\%\cdot\text{K}^{-1}$.

For convenience of comparison, frequency dependence of $S_{Bol}$ can be written as:

$$S_{Bol} = A/f, \tag{4}$$

where $A$ is the dimension factor calculated from $A/f = \Delta V$ for light modulation frequency $f = 10\,\text{Hz}$ and LED radiation power $P = 200\,\text{mW}$ with the fixed external temperature and LIG detector resistance.

Curve $S_{\text{Bol}}(f)$ calculated using expression (4) demonstrates (Figure 5) that $A$ can be used only for $f \leq 45\,\text{Hz}$, i.e. in the frequency range where the bolometric mechanism dominates. With further increase in the modulation frequency, $\Delta V$ is higher than $S_{\text{Bol}}(f)$ by more than two orders of magnitude. The difference in experimental and calculated $\Delta V(f)$ and $S_{\text{Bol}}(f)$ at $f > 45\,\text{Hz}$ can be attributed to the manifestation of photoconductivity resulting from carrier variation, for example, via the „photogating" effect [52]. Note that the photovoltaic effect at the p–n-junction (barrier-layer photo-EMF) in the LIG detector in this system configuration was not observed within the experiment error. This, for example, is evidenced by the independence of the LIG resistance on the current direction in the measurement circuit.

Measurements of $\Delta V(\varphi)$ have shown that at the light incidence angles $\varphi \leq \pm 30^\circ$ relative to normal to the meander surface, decrease in the LIG detector photosensitivity was not higher that $\sim 5\,\%$. Thus, LIG's porous structure provides quite effective light absorption at different angles. The minimum or threshold emitter power detected by the LIG detector is $P_{\min} = \vartheta dP/dR = 0.16\,\%/\text{W}$, where $\vartheta \approx 0.4\,\Omega$ is the standard deviation of the detector resistance without exposure and at full laser power $dR/dP \sim -410\,\Omega/\text{W}$ [51]. The obtained $P_{\min}$ is by an order of magnitude lower than the values typical of monolayer and multilayer graphene [9], but is comparable with data, for example, for nano-composite $MoS_2$ films with high $\beta$ [24,73].

Thus, the LIG detector sensitivity is limited by the interaction between the material and environment and by the carrier mobility. To achieve the properties close to the graphene variables, further optimization is required. For example, improvement of the synthesis technique, selecting the best thickness of the LIG layer itself and of the substrate, and using protective and alloy coatings.

## Conclusion

The study demonstrates that LIG synthesized via polyimide film pyrolysis by continuous $CO_2$ laser is a promising material for creating fast-response visible and IR electromagnetic radiation detectors. It is shown that LIG displays semiconductor properties with an activation energy on the order of 5 meV and carrier mobility of $4300\,\text{cm}^2/(\text{V}\cdot\text{s})$. Thermal resistance coefficient of LIG is approximately 0.05 %/K and 0.15 %/K at 293 K and 200 K, respectively. Porous structure of LIG provides effective light absorption at light incidence angles up to $\pm 30^\circ$ to normal.

Meander-shaped IR detector with thin film copper contacts was made from LIG film. Spectral dependence of detector sensitivity within $0.5 < \lambda < 21\,\mu\text{m}$ is formed by the globar radiation spectrum with features attributed to light absorption by atmospheric $H_2O$ and $CO_2$ vapors, as well as to refractive index dispersion of the optical system prisms.

In the sensitivity maximum region, the LIG detector signal is approximately $10^2 - 10^3$ times lower than that of the industrial uncooled metal bolometer. However, compared with industrial thermal detectors, the LIG detector can be used in a frequency range up to 10 kHz. Frequency dependence of the LIG detector signal is determined by two mechanisms: 1) „barrier effect"– low frequency (below 45 Hz) bolometric effect associated with LIG film heating via light absorption; 2) „photogating effect" — an effect associated with photoinduced variation of free carrier concentration and mobility (at frequencies on the order of and higher than 10 kHz).

Maximum sensitivity of the LIG detector was about 0.16 %/W, which is lower by more than an order of magnitude than the values typical of monolayer and multilayer graphene. Nevertheless, less easy-to-fabricate LIG films can be potentially used in creating flexible fast-response near-IR and mid-IR detectors. The obtained performance of the LIG detector make it possible to recommend it for using in various low-cost and compact consumer and specialized electronics devices.

### Funding

The study was performed under the state order of the Ministry of Education of the Russian Federation for the Institute of Metal Physics, Ural Branch of the Russian Academy of Sciences (№ 1022040600237-3-1.3.2). Some experiments were carried out using the equipment provided by the Shared Research Facility „Center of Physical and Physicochemical Methods of Analysis and Study of the Properties and Surface Characteristics of Nanostructures, Materials, and Products" of the Udmurt Federal Research Center, Ural Branch of RAS.

### Conflict of interest

The authors declare no conflict of interest.

## References

[1] K.S. Novoselov, A.K. Geim, S.V. Morozov, Da Jiang, Ya. Zhang, S.V. Dubonos, I.V. Grigorieva, A.A. Fetisov. Science, **306**, 666 (2004). DOI: 10.1126/science.1102896

[2] D.R. Cooper, B. D'Anjou, N. Ghattamaneni, B. Harack, M. Hilke, A. Horth, N. Majlis, M. Massicotte, L. Vandsburger, E. Whiteway. Intern. Schol. Research Notic., **2012** (1), 501686 (2012). DOI: 10.5402/2012/501686

[3] V. Singh, D. Joung, L. Zhai, S. Das, S.I. Khondaker, S. Seal. Prog. Mater. Sci., **56**, 1178 (2011). DOI: 10.1016/J.PMATSCI.2011.03.003

[4] P.B. Sorokin, L.A. Chernozatonskii. Phys. Usp., **56**, 105 (2013). DOI: 10.3367/UFNe.0183.201302a.0113

[5] A.C. Ferrari, J.C. Meyer, V. Scardaci, C. Casiraghi, M. Lazzeri, F. Mauri, S. Piscanec, D. Jiang, K.S. Novoselov, S. Roth, A.K. Geim. Phys. Rev. Lett., **97**, 187401 (2006). DOI: 10.1103/PhysRevLett.97.187401
[6] A.V. Klekachev, A. Nourbakhsh, I. Asselberghs, A.L. Stesmans, M.M. Heyns, S. De Gendt. Electrochem. Soc. Inter., **22** (1), 63 (2013). DOI: 10.1149/2.F07131if
[7] F.H.L. Koppens, T. Mueller, Ph. Avouris, A.C. Ferrari, M.S. Vitiello, M. Polini. Nat. Nanotechnol., **9** (10), 780 (2014). DOI: 10.1038/nnano.2014.215
[8] C.W.J. Beenakker. Rev. Mod. Phys., **80**, 1337 (2008). DOI: 10.1103/RevModPhys.80.1337
[9] Xu Du, D.E. Prober, H. Vora, C. Mckitterick. Graphene 2D Mater., **1**, 1 (2014). DOI: 10.2478/gpe-2014-0001
[10] Y. Xie, M. Han, R. Wang, H. Zobeiri, X. Deng, P. Zhang, X. Wang. ACS Nano, **13**, 5385 (2019). DOI: 10.1021/acsnano.9b00031
[11] A.L. Gorkina, E.P. Gilstein, A.G. Nasibulin, A.P. Tsapenko, Y.G. Gladush. *Infrared radiation detector based on single-layered carbon nanotubes and graphene* (Patent RU162342U1, 2016)
[12] J.E. Elwood, K.S. Ashok. *Thermal detectors using graphene and oxides of graphene and methods of making the same* (Patent US 10937914 (B1), 2021)
[13] R.G. Zonov, K.G. Mikheev, A.A. Chulkina, I.A. Zlobin, G.M. Mikheev. Diamond Related Mater., **148**, 111409 (2024). DOI: 10.1016/j.diamond.2024.111409
[14] S. Evlashin, P. Dyakonov, R. Khmelnitsky, S. Dagesyan, A. Klokov, A. Sharkov, P. Timashev, S. Minaeva, K. Maslakov, S. Svyakhovskiy, N. Suetin. ACS Appl. Mater. Interf., **8**, 28880 (2016). DOI: 10.1021/acsami.6b10145
[15] J. Lin, Z. Peng, Y. Liu, F. Ruiz-Zepeda, R. Ye, E.L.G. Samuel, M.J. Yacaman, B.I. Yakobson, J.M. Tour. Nat. Commun., **5**, 5714 (2014). DOI: 10.1038/ncomms6714
[16] A. Bianco, H.M. Cheng, T. Enoki, Y. Gogotsi, R.H. Hurt, N. Koratkar, T. Kyotani, M. Monthioux, C.R. Park, J.M.D. Tascon, J. Zhang. Carbon, **65**, 1 (2013). DOI: 10.1016/j.carbon.2013.08.038
[17] Y. Guo, C. Zhang, Y. Chen, Z. Nie. Nanomaterials, **12**, 2336 (2022). DOI: 10.3390/nano12142336
[18] L. Lan, X. Le, H. Dong, J. Xie, Y. Ying, J. Ping. Biosens. Bioelectron., **165**, 112360 (2020). DOI: 10.1016/j.bios.2020.112360
[19] M.G. Stanford, C. Zhang, J.D. Fowlkes, A. Hoffman, I.N. Ivanov, P.D. Rack, J.M. Tour, A. Ho, I.N. Ivanov, P.D. Rack, J.M. Tour. ACS Appl. Mater. Interfaces., **12**, 10902 (2020). DOI: 10.1021/acsami.0c01377
[20] H. Wang, H. Wang, Y. Wang, X. Su, C. Wang, M. Zhang, M. Jian, K. Xia, X. Liang, H. Lu, S. Li, Y. Zhang, Laser. ACS Nano, **14**, 3219 (2020). DOI: 10.1021/acsnano.9b08638
[21] M. Dosi, I. Lau, Y. Zhuang, D.S.A. Simakov, M.W. Fowler, M.A. Pope. ACS Appl. Mater. Interfaces, **11**, 6166 (2019). DOI: 10.1021/acsami.8b22310
[22] M.G. Stanford, K. Yang, Y. Chyan, C. Kittrell, J.M. Tour. ACS Nano., **13**, 3474 (2019). DOI: 10.1021/acsnano.8b09622
[23] N.T. Garland, E.S. McLamore, N.D. Cavallaro, D. Mendivelso-Perez, E.A. Smith, D. Jing, J.C. Claussen. ACS Appl. Mater. Interfaces, **10**, 39124 (2018). DOI: 10.1021/acsami.8b10991
[24] W. Yan, W. Yan, T. Chen, J. Xu, Q. Tian, D. Ho. ACS Appl. Nano Mater., **3**, 2545 (2020). DOI: 10.1021/acsanm.9b02614
[25] C. Yi, Y. Hou, K. He, W. Li, N. Li, Z. Wang, B. Yang, S. Xu, H. Wang, C. Gao, Z. Wang, G. Gu, Z. Wang, L. Wei, C. Yang, M. Chen. ACS Appl. Mater. Interfaces, **12**, 19563 (2020). DOI: 10.1021/acsami.0c02774
[26] G. Li, W.-C. Law, K.C. Chan. Green Chem., **20**, 3689 (2018). DOI: 10.1039/C8GC01347K
[27] L. Huang, L. Ling, J. Su, Y. Song, Z. Wang, B.Z. Tang, P. Westerhoff, R. Ye. ACS Appl. Mater. Interfaces, **12**, 51864 (2020). DOI: 10.1021/acsami.0c16596
[28] C.M. Tittle, D. Yilman, M.A. Pope, C.J. Backhouse. Adv. Mater. Technol., **3**, 1700207 (2018). DOI: 10.1002/admt.201700207
[29] L. Cheng, W. Guo, X. Cao, Y. Dou, L. Huang, Y. Song, J. Su, Z. Zeng, R. Ye. Mater. Chem. Front., **5**, 4874 (2021). DOI: 10.1039/d1qm00437a
[30] J. Li, Z. Jing, F. Zha, Y. Yang, Q. Wang, Z. Lei. ACS Appl. Mater. Interfaces, **6**, 8868 (2014). DOI: 10.1021/am5015937
[31] T. Darmanin, F. Guittard. J. Mater. Chem. A, **4**, 3197 (2016). DOI: 10.1039/C5TA09253A
[32] C.R. Szczepanski, F. Guittard, T. Darmanin. Adv. Colloid Interface Sci., **241**, 37 (2017). DOI: 10.1016/j.cis.2017.01.002
[33] R. Ye, D.K. James, J.M. Tour. Adv. Mater., **31**, 1803621 (2019). DOI: 10.1002/adma.201803621
[34] W. Song, J. Zhu, B. Gan, S. Zhao, H. Wang, C. Li, J. Wang. Small, **14**, 1702249 (2018). DOI: 10.1002/smll.201702249
[35] W. Ma, J. Zhu, Z. Wang, W. Song, G. Cao. Mater. Today Energy, **18**, 100569 (2020). DOI: 10.1016/j.mtener.2020.100569
[36] J. Cai, C. Lv, A. Watanabe. J. Mater. Chem. A, **4**, 1671 (2016). DOI: 10.1039/C5TA09450J
[37] P. Zaccagnini, D. di Giovanni, M.G. Gomez, S. Passerini, A. Varzi, A. Lamberti. Electrochim. Acta, **357**, 136838 (2020). DOI: 10.1016/j.electacta.2020.136838
[38] D. Yang, C. Bock. J. Power Sources, **337**, 73 (2017). DOI: 10.1016/j.jpowsour.2016.10.108
[39] Y. Wang, Y. Zhao, L. Qu. J. Energy Chem., **59**, 642 (2021). DOI: 10.1016/j.jechem.2020.12.002
[40] J. Yi, J. Chen, Z. Yang, Y. Dai, W. Li, J. Cui, F. Ciucci, Z. Lu, C. Yang, Adv. Energy Mater., **9**, 1901796 (2019). DOI: 10.1002/aenm.201901796
[41] R. Ye, Z. Peng, T. Wang, Y. Xu, J. Zhang, Y. Li, L.G. Nilewski, J. Lin, J.M. Tour. ACS Nano, **9**, 9244 (2015). DOI: 10.1021/acsnano.5b04138
[42] D.X. Luong, K. Yang, J. Yoon, S.P. Singh, T. Wang, C.J. Arnusch, J.M. Tour. ACS Nano, **13**, 2579 (2019). DOI: 10.1021/acsnano.8b09626
[43] Y. Chyan, R. Ye, Y. Li, S.P. Singh, C.J. Arnusch, J.M. Tour, ACS Nano, **12**, 2176 (2018). DOI: 10.1021/acsnano.7b08539
[44] L. Huang, S. Xu, Z. Wang, K. Xue, J. Su, Y. Song, S. Chen, C. Zhu, B.Z. Tang, R. Ye. ACS Nano, **14**, 12045 (2020). DOI: 10.1021/acsnano.0c05330
[45] R.M. Torrente-Rodríguez, H. Lukas, J. Tu, J. Min, Y. Yang, C. Xu, H.B. Rossiter, W. Gao. Matter, **3**, 1981 (2020). DOI: 10.1016/j.matt.2020.09.027
[46] K.G. Mikheev, R.G. Zonov, T.N. Mogileva, A.E. Fateev, G.M. Mikheev. Opt. Laser Technol., **141**, 107143 (2021). DOI: 10.1016/j.optlastec.2021.107143
[47] X. Yu, N. Li, S. Zhang, C. Liu, L. Chen, S. Han, Y. Song, M. Han, Z. Wang. J. Power Sources, **478**, 229075 (2020). DOI: 10.1016/j.jpowsour.2020.229075

[48] K.G. Mikheev, R.G. Zonov, D.L. Bulatov, A.V. Syugaev, G.M. Mikheev. Technical Physics Letters, **50** (10), 51 (2024). DOI: 10.61011/TPL.2024.10.60118.19976
[49] K.G. Mikheev, A.V. Syugaev, R.G. Zonov, D.L. Bulatov, G.M. Mikheev. Phys. Solid State, **65** (2), 347 (2023). DOI: 10.21883/PSS.2023.02.55422.529
[50] K.G. Mikheev, R.G. Zonov, D.L. Bulatov, A.E. Fateev, G.M. Mikheev. Tech. Phys. Lett., **46**, 458 (2020). DOI: 10.1134/S1063785020050119
[51] C. Zhang, Y. Xie, H. Deng, T. Tumlin, C. Zhang, J.W. Su, P. Yu, J. Lin. Small, **13**, 1604197 (2017). DOI: 10.1002/smll.201604197
[52] Yu.P. Sukhorukov, A.V. Telegin, K.G. Mikheev, R.G. Zonov, L.I. Naumova, G.M. Mikheev. Opt. Mater., **133**, 112957 (2022). DOI: 10.1016/j.optmat.2022.112957
[53] R.G. Zonov, K.G. Mikheev, D.L. Bulatov, T.N. Mogileva, A.V. Syugaev, G.M. Mikheev. Diam. Relat. Mater., **157**, 112529 (2025). DOI: 10.1016/j.diamond.2025.112529
[54] K.G. Mikheev, A.E. Fateev, R.G. Zonov, D.L. Bulatov, G.M. Mikheev. Journal of Physics: Conference Series. IOP Publishing. **1695** (1), 012113 (2020). DOI: 10.1088/1742-6596/1695/1/012113
[55] A.V. Kuksin, A.Y. Gerasimenko, Y.P. Shaman, E.P. Kitsyuk, A.A. Shamanaev, A.V. Sysa, E.M. Eganova, M.M. Slepchenkov, M.V. Poliakov, A.A. Pavlov, O.E. Glukhova. Appl. Surf. Sci., **664**, 160222 (2024). DOI: 10.1016/j.apsusc.2024.160222
[56] N.P. Nekrasov, D.T. Murashko, P.N. Vasilevsky, A.Y. Gerasimenko, V.K. Nevolin, I.I. Bobrinetskiy. Semiconductors, **58**, 1109 (2024). DOI: 10.1134/S1063782624700131
[57] J. Zhai, Z. Yu, J. Hu. Manuf. Process, **146**, 211 (2025). DOI: 10.1016/j.jmapro.2025.05.001
[58] N.N. Nghia, D.T.C. Minh, N.H. Hieu. Microchem. J., **213**, 113713 (2025). DOI: 10.1016/j.microc.2025.113713
[59] K.G. Mikheev, R.G. Zonov, A.V. Syugaev, D.L. Bulatov, G.M. Mikheev. Physics of the Solid State, **64** (5), 579 (2022). DOI: 10.21883/PSS.2022.05.53520.277
[60] Z. Yin, S. Chen, C. Hu, J. Li, X. Yang. Opt. Laser Technol., **176**, 110998 (2024). DOI: 10.1016/j.optlastec.2024.110998
[61] X. Li, W. Cai, K.S. Teh, M. Qi, X. Zang, X. Ding, Y. Cui, Y. Xie, Y. Wu, H. Ma, Z. Zhou, Q.A. Huang, J. Ye, L. Lin. ACS Appl. Mater. Interfaces, **10**, 26357 (2018). DOI: 10.1021/acsami.8b10301
[62] A. Rabti, S. Baachaoui, M. Zouari, N. Raouafi. J. Pharm. Biomed. Anal. Open, **5**, 100069 (2025). DOI: 10.1016/j.jpbao.2025.100069
[63] I.V. Antonets, E.A. Golubev, V.G. Shavrov, V.I. Shcheglov. J. Radio Electron., **3**, 1684 (2020). DOI: 10.30898/1684-1719.2020.3.7
[64] P.L. Richards. J. Appl. Phys., **76** (1), 1 (1994). DOI: 10.1063/1.357128
[65] B.N. Formozov. *Aerokosmicheskie fotopriemnye ustroistva v vidimom i infrakrasnom diapazonakh* (SPbGUAP, SPb, 2002) (in Russian)
[66] A.N.Aleksandrov, V.A.Nikitin. UFN, **56** (5), 3 (1955) (in Russian).
[67] D.S.L. Abergel, V. Apalkov, J. Berashevich, K. Ziegler, T. Chakraborty. Adv. Phys., **59** (4), 261 (2010). DOI: 10.1080/00018732.2010.487978
[68] A.V.Eletsky, I.M. Iskandarova, A.A.Knizhnik, D.N.Krasikov. UFN, **181** (3), 233 (2011) (in Russian). DOI: 10.3367/UFNe.0181.201103a.0233
[69] R.A.Brazhe, A.I.Kochaev, R.M.Meftakhutdinov. *Grafeny i ikh fizicheskie svoistva* (UlGTU, Ulyanovsk, 2016) (in Russian)
[70] J.J. Bae, J.H. Yoon, S. Jeong, B.H. Moon, J.T. Han, H.J. Jeong, G.W. Lee, H.R. Hwang, Y.H. Lee, S.Y. Jeong, S.C. Lim. Nanoscale, **7**, 15695 (2015). DOI: 10.1039/C5NR04039F
[71] J. Yan, M.H. Kim, J.A. Elle, A.B. Sushkov, G.S. Jenkins, H.W.M. Milchberg, M.S. Fuhrer, H.D. Drew. Nat. Nanotechnol., **7**, 472 (2012). DOI: 10.1038/nnano.2012.88
[72] K.G. Mikheev, R.G. Zonov, N.V. Chuchkalov, G.M. Mikheev. Physics of the Solid State, **66** (2), 268 (2024). DOI: 10.61011/PSS.2024.02.57924.5
[73] Q. Wang, Y. Wu, X. Deng, L. Xiang, K. Xu, Y. Li, Y. Xie. Nanomaterials, **12**, 495 (2022). DOI: 10.3390/nano12030495

*Translated by E.Ilyinskaya*